

Parametric study on the lateral strength of URM wall, retrofitted using ECC mortar

Alireza Namayandeh Niasar^{1a}, Farshid Jandaghi Alaei^{*1} and Sohail Majid Zamani^{2b}

¹Department of Civil Engineering, Shahrood University of Technology, Shahrood, Iran

²Structural Engineering Dept., BHRC, Tehran, Iran

(Received September 12, 2019, Revised December 30, 2019, Accepted January 18, 2020)

Abstract. In this paper, the effect of Engineered Cementitious Composites (ECC) on the lateral strength of a bearing unreinforced Masonry (URM) wall, was experimentally and numerically investigated. Two half scale solid walls were constructed and were tested under quasi-static lateral loading. The first specimen was an un-retrofitted masonry wall (reference wall) while the second one was retrofitted by ECC mortar connected to the wall foundation via steel rebar dowels. The effect of pre-compression level, ECC layer thickness and one or double-side retrofitting on the URM wall lateral strength was numerically investigated. The validation of the numerical model was carried out from the experimental results. The results indicated that the application of ECC layer increases the wall lateral strength and the level of increment depends on the above mentioned parameters. Increasing pre-compression levels and the lack of connection between the ECC layer and the wall foundation reduces the influence of the ECC mortar on the wall lateral strength. In addition, the wall failure mode changes from flexure to the toe-crushing behavior. Furthermore, in the case of ECC layer connected to the wall foundation, the ECC layer thickness and double-side retrofitting showed a significant effect on the wall lateral strength. Finally, a simple method for estimating the lateral strength of retrofitted masonry walls is presented. The results of this method is in good agreement with the numerical results.

Keywords: retrofitting; engineered cementitious composites; earthquake; quasi-static lateral loading; numerical study

1. Introduction

A significant number of unreinforced masonry (URM) buildings have been constructed around the world. Due to the lack of design, poor quality of materials and construction, most of these buildings are vulnerable against earthquakes (Ural 2013, Bilgin and Huta, 2018). Therefore, different seismic rehabilitation methods have always been considered by researchers. On the other hand, the occurrence of earthquakes in different parts of the world may cause damages in these buildings. URM walls in-plane failure modes are classified as deformation-controlled (bed-joint sliding and rocking behavior) or force-controlled (diagonal tension cracking and toe compression) modes (ASCE/41-17 2017, Vanin and Foraboschi 2012). Several methods have been taken into account by researchers to improve the behavior of the masonry walls under seismic loads. One of the traditional methods includes coating the walls with Reinforced Concrete (RC) layers or welded wire mesh and mortar. In this method, the wall is retrofitted by a steel mesh and a layer of cement mortar of 50 to 100mm thickness (Kadam *et al.* 2014, Ghiassi *et al.* 2011). Furthermore, Darbhanzi *et al.* (2018) have introduced using

steel strips (diagonal and vertical) as another traditional method for retrofitting masonry walls. The results have shown these methods can improve the retrofitted wall performance, especially the wall lateral strength. The use of polymer materials such as Fiber Reinforced Polymers (FRP) are known as novel methods. FRP is one of the well-known methods used to increase the strength and ductility of the in-plane bearing masonry walls (Nezhad *et al.* 2016, Luccioni and Rougier 2011, ElGawady *et al.* 2007, ACI/440.7R 2010, Basilio *et al.* 2014). The use of polymeric materials in the form of mesh with cement based mortar is another method used to retrofit the masonry walls. Popa *et al.* (2016) have investigated the effect of FRP grids bonded by cement mortar on the behavior of the squat masonry walls. The results of this research have indicated that applying the fibre reinforced cement mortar does not effectively improve the hysteretic behavior and only prevents imposing the early damage. Regarding the type of mortar and polymer materials, the following types of materials have been tested by other researchers: Textile Reinforced Mortar (TRM), Textile Reinforced Concrete (TRC), Fabric-Reinforced Cementitious Matrix (FRCM), Cementitious Matrix-Grid (CMG) or Inorganic Matrix-Grid (IMG) composite (Maso *et al.* 2014, Yardim and Lalaj 2016, Bernat-Maso *et al.* 2015, Triantafillou 2011, Carozzi *et al.* 2014, Ismail *et al.* 2018, Bertolesi *et al.* 2014, Carozzi *et al.* 2018). In the present research, Engineered Cementitious Composites (ECC) has been used for retrofitting the bearing URM walls. ECC is a part of a larger class of materials, called Fiber Reinforced Concrete (FRC).

*Corresponding author, Professor, Ph. D

E-mail: Fjalaei@shahroodut.ac.ir

^aPh. D. Student

^bProfessor

Traditional unreinforced cementitious materials do not possess significant tensile strain (typically less than 0.015% strain) and strength capacity (typically less than 3.5 MPa). ECC is an innovative composite material which exhibit pseudo-strain hardening in tension. ECC is comprised of a Portland cement paste or mortar matrix with a low volume fraction of fibers such as ultrahigh molecular weight polyethylene (UHMWPE) or polyvinyl alcohol (PVA) fibers. The fibers in ECC give the material tensile strain capacities ranging from 0.5 to 6% and tensile strengths from 2 to 8 MPa (Kesner and Billington 2004). Several studies have been carried out on the effect of this type of material on the performance of concrete structures and masonry infilled. Generally, it has been shown that ECC has a significant role in improving the behavior of retrofitted structures (Kyriakides and Billington 2014, Dehghani *et al.* 2015, Liang and Xing 2018, Kota *et al.* 2019, Lin *et al.* 2016, AL-Gemeel *et al.* 2018, Maalej *et al.* 2010, Singh *et al.* 2017, Hung and Chen 2016).

Yi-Wei Lin *et al.* (2014) have investigated the effect of ECC mortar on the behavior of the brick URM wallettes. The results of research have indicated that ECC mortar is effective at enhancing both the in-plane strength and the pseudo-ductility of URM wallettes. It has also been shown that with increasing the masonry wallette thickness, the bonding between masonry wallette and ECC layer is decreased.

Mingke Deng and Shuo Yang (2018) have investigated the performance of URM walls retrofitted with ECC mortar. In their research, six half scale specimens including un-retrofitted and retrofitted walls were constructed and with static cyclic lateral loading tested. Two walls were retrofitted by applying ECC mortar with strip pattern whereas, the other two were completely retrofitted by a constant thickness of ECC mortar. The results of this research indicated that these retrofitting techniques can effectively improve the lateral strength and the displacement ductility of URM walls.

Although the results of above research indicate that this retrofitting technique can effectively improve the lateral strength of URM walls, there are still some questions about the effect of the following main parameters on the lateral capacity of the retrofitted URM wall.

- selection of bed joint sliding failure mode for the un-retrofitted wall,
- the way of ECC layer connection to the URM wall foundation, the effect of the ECC mortar applied on one side of the wall,
- changes in compressive stress due to gravity load and changes the thickness of the ECC layer.

In the present study, these parameters, is experimentally and numerically investigated. Also, based on the obtained results, a model for calculating the shear capacity of this type of structure has been proposed.

2. Experimental study

2.1 Experimental program

In this study, the experimental program was performed

in two stages: tests on constituent materials and URM wall specimens.

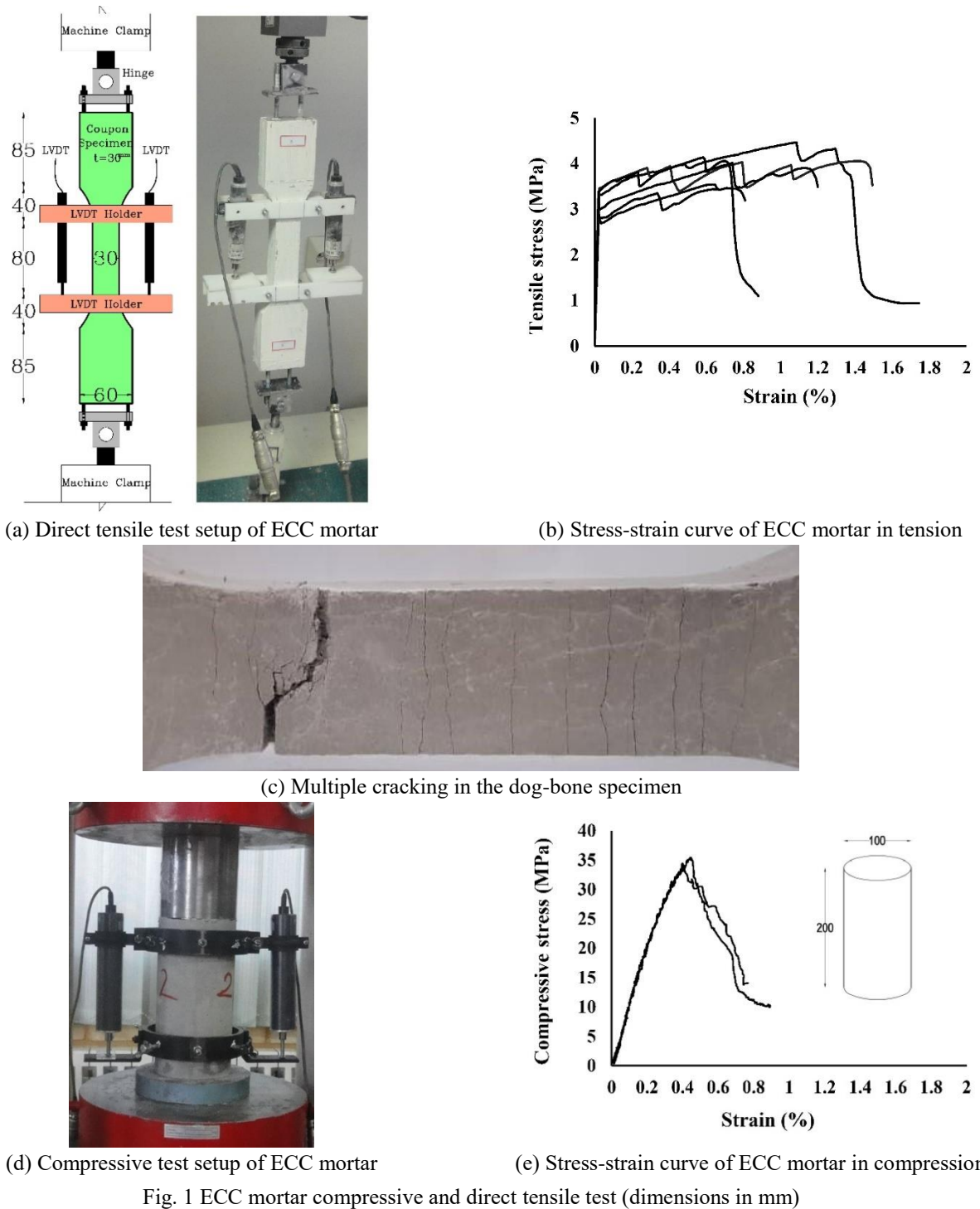
2.1.1 Materials experimental program

- ECC materials

ECC mortar is a typical fiber reinforced cementitious composite that shows an obvious strain-hardening characteristic under tension and a good toughness characteristic under compression. To investigate these behaviors, direct tensile and compression test have been performed. The ECC materials consisted of ordinary Portland cement, fly ash (class F) and fine silica (maximum grain size 0.15 mm), water proportions of 1: 2: 0.70 and 0.75, respectively. High-range water-reducing admixture content is 3.93 kg/m³ and the volume content of polyvinyl alcohol (PVA) fibers is 2%. The tensile strength, Young's modulus, elongation, density, diameter and length of PVA fibers are 1600 MPa, 42.8 GPa, 6%, 1.3 gr/cm³, 39 μ m and 8 mm, respectively.

To study the tensile behavior of ECC, uniaxial tensile tests were conducted on six dog-bone shaped specimens. The thickness of the specimens was 30mm and the other dimensions of the specimens can be found in Fig. 1a. To make ECC mortar, dry materials were first mixed together. Then water and superplasticizer were gradually added. After the preparing the paste, PVA fibers were added. ECC mortar was cast in dog bone mold and cured for 28 days before testing. A universal machine with a capacity of 50 kN was used for testing. As shown in Fig. 1a, for measuring the longitudinal deformation of the specimens under tensile force, two Linear Variable Differential Transformers (LVDTs) were used on both sides of the specimens. The measured distance between two points of the specimen was 80 mm. According to JSCE-2008 (2008), the specimens were tested under displacement control at a rate of 0.5mm/min. The test results are presented in Fig. 1(b) and 1(c). After first cracking, the stress continues to rise with the formation of multiple cracking in the ECC mortar, which contributes to the increase of the inelastic strain. After the peak stress is reached, a localized crack occurs, leading to the failure of the specimen. The specimens after failure are shown in Fig. 1(c). The average first cracking strength and ultimate tensile strength is 3.25 MPa and 3.8 MPa, respectively. The average ultimate tensile strain ranges from 0.68% to 1.56%, with an average value of 1.02%. This variation of the tensile strain can be attributed to the random matrix flaws and random fibers distribution, which combine together to determine the number of cracks that can be formed before failure localization occurs.

The compressive strength of ECC was obtained based on two cylindrical specimens with a diameter of 100 mm and a height of 200 mm. In accordance with EN 12390-3 (2009), the specimens were compressed under displacement control at a rate of 0.5mm/min. As shown in Fig. 1(d), the displacement between two points on the specimen was measured by two LVDTs. The distance between two points was 100 mm. The compressive stress-strain curve of the specimens is presented in Fig. 1(e). According this Figure, in the pre-peak stage, specimens behave elastically at the



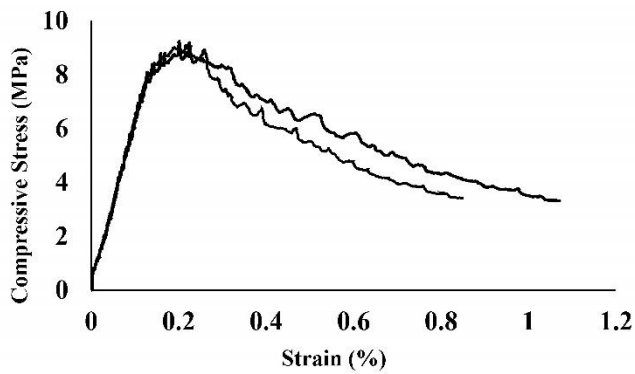
initial stage. After the stress reaches approximately 70% of the peak stress, the Young's modulus starts to reduce, showing nonlinear behavior. At the post-peak stage, the stress drops with cracks propagating. After the inflection point, the stress decreases more slowly with the increase of strain. The average compressive strength and strain are 35 MPa and 0.39%, respectively. The average of the Young's modulus of the ECC at the age of 28 days is 10400 MPa.

The Young's modulus is less than that of conventional concrete with the same compressive strength, which might be due to the absence of coarse aggregates.

- Masonry materials

The mechanical properties of masonry materials including the shear sliding behavior of masonry and the compressive behavior of bricks, cement mortar and masonry prism, were obtained based on triplet shear test and uniaxial compressive tests, respectively. These tests were performed according to ASTM-C 67-14 (2014) and ASTM-C 270-07 (2007).

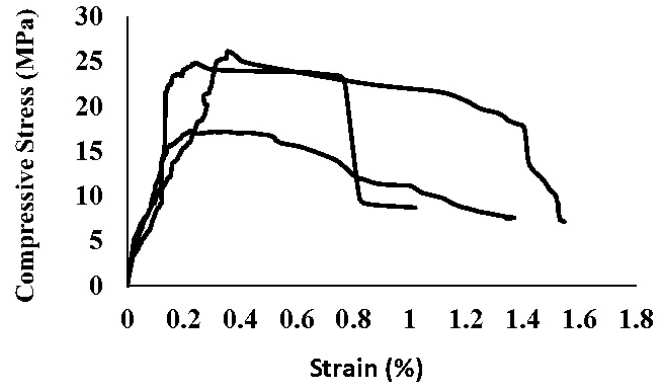
Portland cement type II and quartz sand with maximum aggregate size of 4 mm were used to cast the mortar.



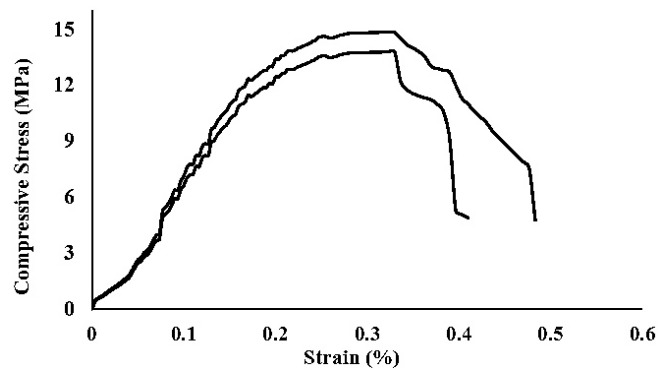
(a) Stress-strain curve of cement mortar in compression



(c) Test setup of prism masonry



(b) Stress-strain curve of brick in compression



(d) Stress-strain curve of prism masonry in compression

Fig. 2 Masonry compressive test

Cement, water and sand with a volume ratio of 1:1.1:5 were mixed. The compressive strength and Young's modulus of mortar was obtained based on ASTM C469-14 (2002). Three cylindrical specimens with a diameter of 100 mm and a height of 200 mm were compressed under displacement control at a rate of 0.5 mm/min. As shown in Fig. 1(d), the displacement between two points on the specimen was measured by two LVDTs. The distance between two points was 130mm. The compressive stress-strain curve of the specimens is presented in Fig. 2(a). The average compressive strength and Young's modulus of mortar were 9.11MPa and 6323MPa, respectively. The results indicated that the tested mortar was similar to type "N" mortar stated in ASTM-C270-07 (2007).

In this research, clay bricks with dimensions of 215 × 110 × 65 mm (length × width × thickness) were used. To determine the bricks compressive behavior, three cylindrical specimens with a diameter of 54mm and a height of 88mm were first prepared with core drilling. Then, as shown in Fig. 1(d), specimens were loaded under compression, similar to specimens of ECC mortar. The spacing between two fix point of each LVDT was 40mm. The results of the experiments are presented in Fig. 2(b). The average compressive strength and Young's modulus of mortar were 22.3 MPa and 19400 MPa, respectively.

In order to investigate the compressive behavior of masonry elements, masonry prisms were constructed and tested under axial compression according to ASTM C1314-16 (2016). Two specimens were tested. All prisms included

five bricks bonded together by mortar joints with a thickness of 10 mm. The bearing surfaces of the top and the bottom bricks were grinded before prisms construction to avoid premature failure due to the uneven surfaces of bricks. The ratio of prism height to the least lateral dimension of prism was 2.2. As shown in Fig. 2(c), the load was applied by displacement control at a rate of 0.5 mm/min and the compressive displacement of the prism was measured using an LVDT with a gauge length of 150 mm. The compressive stress-strain curve of the specimens is presented in Fig. 2(d). The average compressive strength and Young's modulus of masonry element were 13.7 MPa and 4900 MPa, respectively.

The procedure described in BS EN1052-3 (2007) was adopted, which is used to evaluate bed joint shear behavior of masonry using triplet specimens. To prepare the test specimens, a series of triplet specimens were constructed by three full bricks and two mortar joints. Nine specimens, three of which for cement mortar bed joint, two for ECC mortar bed joint and the remaining four for cement mortar bed joint with constant confining pressure 0.5 and 1 MPa were tested under displacement control at a rate of 0.5 mm/min. As shown in Fig. 3(a), to measure the displacement of the middle brick, two LVDTs were used on the both sides of the specimen, which is located on the side bricks through a frame made of aluminum. As shown in Fig. 3b, to apply a constant confining pressure, two steel plates were attached to both sides of the specimen and kept in position with four bolts. A uniform confining pressure was

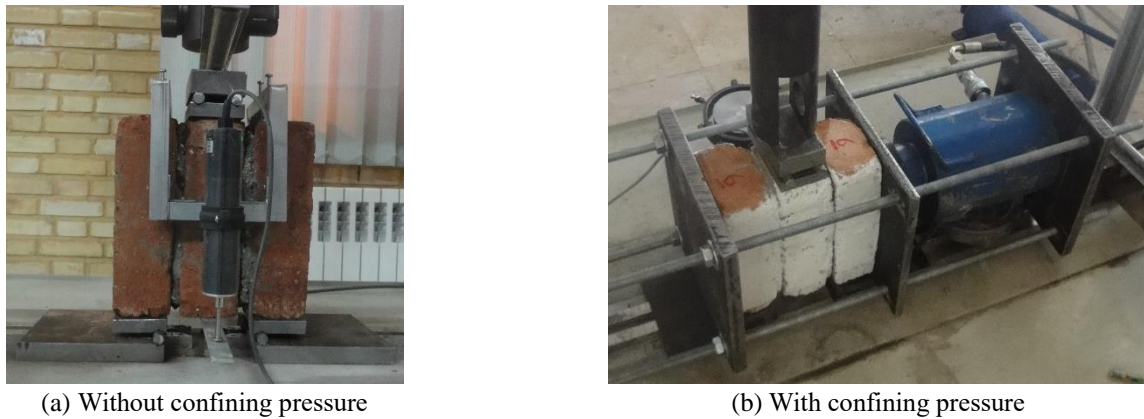


Fig. 3 Triplet test setup

Table 1 Experimental results on triplet test specimen

Specimen number	Mortar of bed joint	σ ¹	V_{\max} ² (kN)	τ_{\max} ³ (MPa)
1	1	Cement mortar	0	10
2	2	Cement mortar	0	8
3	3	Cement mortar	0	11.6
4	4	ECC mortar	0	13.2
5	5	ECC mortar	0	10
6	6	Cement mortar	0.5	32.8
7	7	Cement mortar	0.5	-
8	8	Cement mortar	1	56
9	9	Cement mortar	1	52

Note: 1= normal pre-compression; 2= ultimate shear force; 3= ultimate shear strength

exerted to the specimen using a manually controlled hydraulic jack having a load gauge. When the expected level of pressure was reached, the specimen was ready for the shear test. The experimental test results are presented in Table 1.

The bond strength between the ECC layer and cement mortar with the brick surface was measured on average 0.29 MPa and 0.25 MPa, respectively. The average friction coefficient between cement mortar and brick surface was measured 0.91.

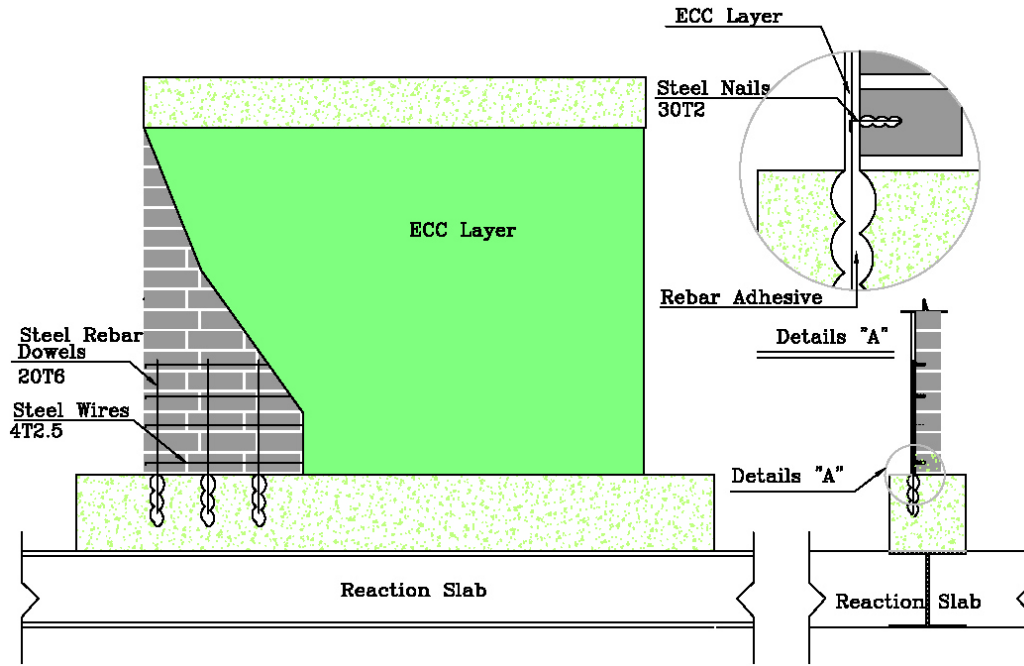
2.1.2 Main specimens experimental program

The wall selected for testing was part of a one-story building. Dimensions of the wall were considered at half scale as 2000 × 1400 × 110 mm (length × height × thickness). The length and height dimensions were selected in such a way that their ratio was between 0.5 and 1, leading to a shear type failure mode (the failure modes of bed joint sliding or diagonal tension). The specimens were made to resemble the construction of masonry buildings in Iran. Two wall specimens were cast and tested. The first specimen was not retrofitted to be the reference wall. The second one was

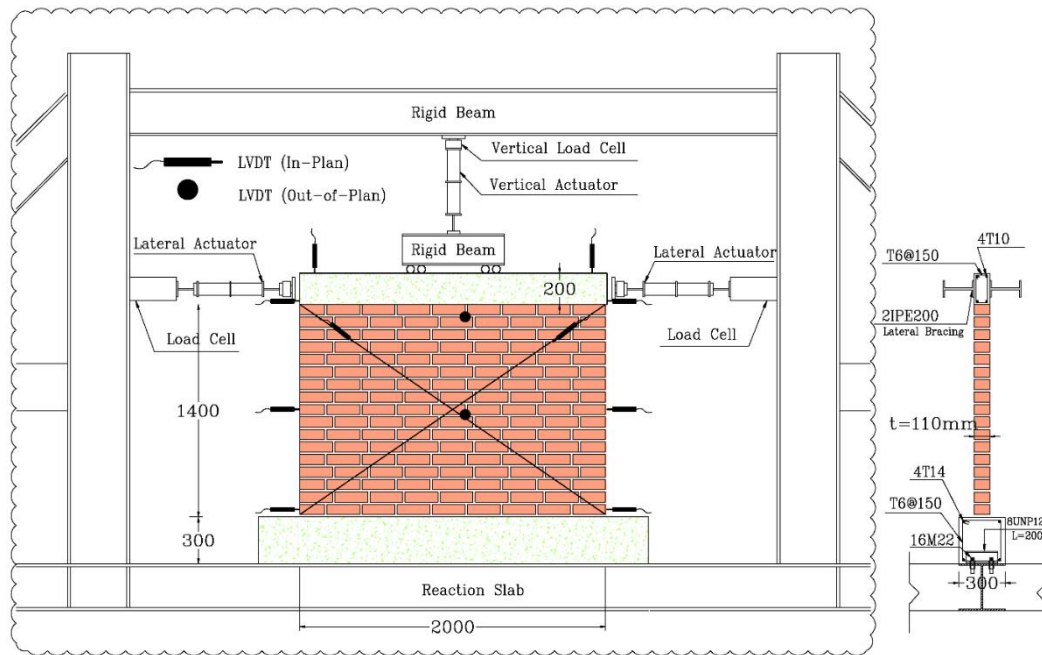
a specimen retrofitted with ECC mortar. The masonry wall was constructed using solid clay bricks bonded with approximately 10mm thickness of mortar joints. Cement, water and sand with a volume ratio of 1:1.1:5 were mixed. Wall specimen sits on a foundation measuring 2500 × 300 × 300 mm (length × width × thickness) and a reinforced concrete beam on the top of wall measuring 2000 × 100 × 100mm (length × width × thickness) is provided to distribute and transfer the loads to the wall. The wall foundation was connected to the strong floor through sixteen bolts (M22). According to Fig. 4(a), the ECC mortar was applied on one side of the specimens. The average thickness of the ECC layer for retrofitted wall was considered to be 15 mm. To connect the ECC layer to the wall foundation, twenty steel rebar dowels were used with a diameter of 6mm and a length of 50 mm. They were anchored in the wall foundation at a depth of 100 mm using special rebar adhesive. Also, to prevent steel rebar dowels buckling, four horizontal steel wires with a diameter of 2.5 mm were used. These wires were connected to the wall through 2 mm diameter steel nails.

- Test setup

As shown in Fig. 4(b), the bearing masonry wall has been supported by a concrete foundation on the laboratory's strong floor. The test loading instruments consisted of two horizontal and a vertical hydraulic actuator, with a capacity of 1000kN and three load cells with a capacity of 100kN. Horizontal and vertical actuators and load cells capacity was calculated based on the estimated load-carrying capacity of the specimens and the vertical load, respectively. During the test, the vertical load was applied by a hydraulic actuator which was monitored to keep its force fixed and constant during the test. The quasi-static cyclic lateral loading was applied to the reinforced concrete beam on the top of the wall, which in turn distributed the force to the specimen. This load was applied manually using two hydraulic actuator and hand pumps. Twelve LVDTs were used to measure vertical, horizontal and diagonal in-plane displacements of the wall. To measure the out-of-plan displacements of the wall, two LVDTs were used. Also, two IPE200 steel sections were installed longitudinally to provide out of plane support for both sides of wall.



(a) Details of retrofitted URM wall



(b) Test setup, loading system, and instrumentation

Fig. 4 Retrofitted specimen experimental details (dimension in mm)

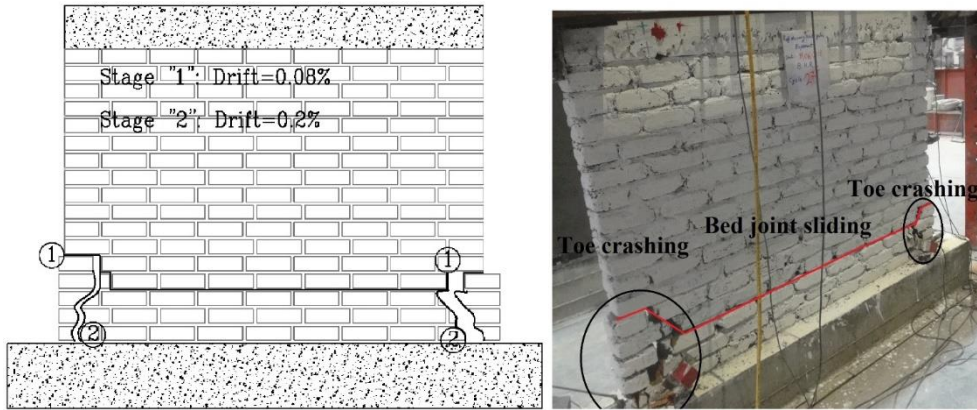
- Loading protocol

The bearing URM wall was simultaneously under vertical and lateral loads. The wall average compression stress due to the vertical load was 0.1MPa. The quasi-static cyclic lateral loading scheme was displacement-controlled. Different quasi-static cyclic lateral loading protocols have been used by researchers (Krawinkler 2009, ISO-16670:2003, 2003, ATC 24, 1992, FEMA-F.461, 2007). These loading patterns are rather similar. As there is no much difference between their energy dissipation demands

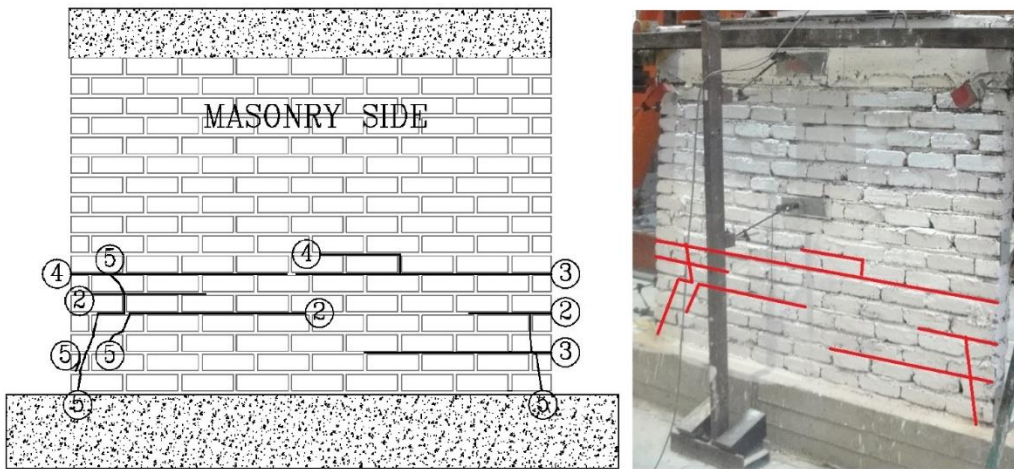
and they are expected to produce a similar performance (Krawinkler 2009)

In this research, the lateral loading pattern developed by FEMA461 (2007) was selected because of its stepwise increasing deformation amplitude. This pattern allows defining more cycles in the small and moderate drift ranges and reducing the number of cycles in larger lateral drifts.

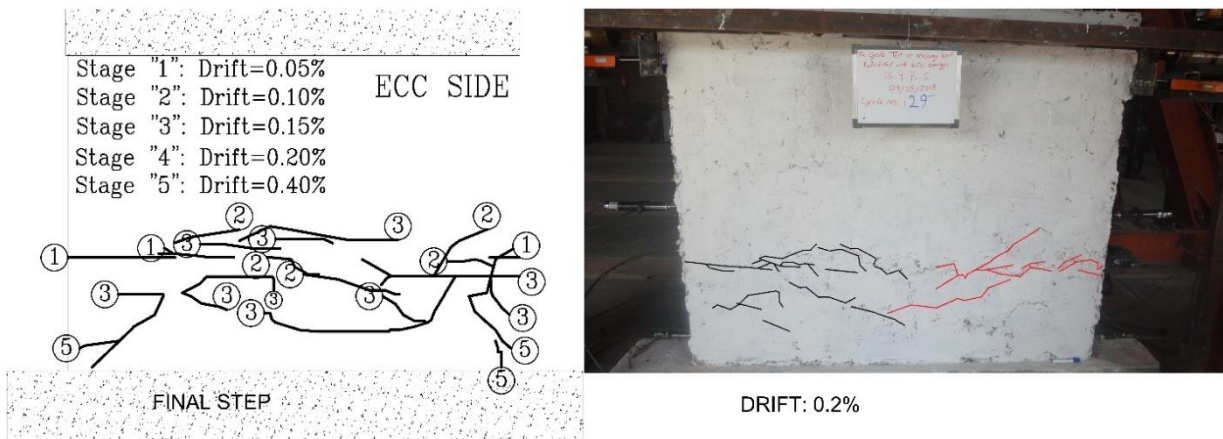
The drift pattern used in the tests consisted of two cycles at each drift level, starting at 0.01% and increasing up to 1.02%, if failure did not occur before.



(a) Reference specimen



(b) Retrofitted specimen (masonry side)



(c) Retrofitted specimen (ECC side)

Fig. 5 Cracking pattern of specimens

-Experimental results

In this section, hysteresis curves, cracking patterns and envelope curve of experiments on the reference and retrofitted URM wall specimens are presented and compared.

The specimens cracking patterns and hysteresis curves are presented in Fig. 5 and 6, respectively.

According to experimental observations of the reference specimen, the wall had a linear behavior up to 0.04% drift,

so that there were no cracks in the wall.

In the drift of 0.08% (stage 1), by increasing the lateral force, sliding along the bed joint mortar occurred. This sliding was observed at the bottom of the wall in the fourth bed joint mortar, about 250mm above the wall foundation. In addition, the wall stiffness decreased whereas the amount of strength did not change. In the drift of 0.2% (stage 2), cracks in the wall toe and in the bricks were observed. The wall shear strength also decreased. At a drift of 0.6%, in

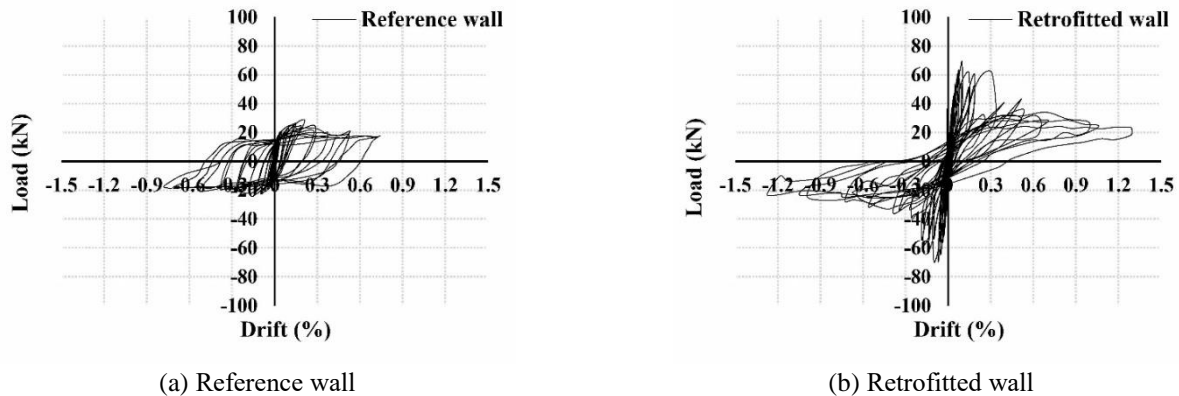


Fig. 6 Hysteresis curve of specimens

addition to the shear strength decrease, the wall was displaced horizontally under constant force and toe crushing was expanded. The amount of wall displacement was measured as 25 mm. In general, the wall failure mode was a combination of bed joint sliding and toe crushing.

The retrofitted specimen had a linear behavior up to 0.04% drift, and no cracks in the ECC layer and wall occurred. As the displacement increased (0.05% drift, stage 1), the cracks appeared at the top of the steel rebar dowels and appeared on the ECC layer. These cracks expanded up gradually to a drift of 0.10% and 0.15% at the surface of the ECC layer (stage 2,3). In other words, multiple cracking phenomena were observed in the ECC layer. With increasing displacement, only the width of the cracks in the ECC layer was grown and moved to the masonry surface. In drift of 0.20%, with increasing the crack width, a decrease in wall strength was observed (stage 4). As the displacement increased (drift of 0.4%), due to the bending failure, the crack width of the ECC layer increased up to 7mm (stage 5). During the test, there was no debonding between the ECC layer and the masonry wall. Although the specimen was loaded up to 1.3% drift, the wall instability was not observed. In the drift of 1%, the bed joint sliding was observed at the top of the steel rebar dowels. In addition, cracking in few bricks was observed in the wall toe. The specimen failure mode was a rocking (flexural behavior) failure mode.

According to Fig. 6, the increase in the strength of the retrofitted specimen is about 2.7 times more than that of the reference wall. In the drift of 0.20%, strength reduction and softening behavior were observed in the retrofitted specimen. Despite the in-plane behavior of the reference wall, the softening behavior was not accompanied with the in-plane intense instability. This was due to the integrity of the masonry units resulting from the presence of ECC layer.

3. Numerical modeling

The numerical model for this study was developed using the software ABAQUS 6.14 (2013). In the numerical analysis only monotonic loading was considered, as the focus here is on the parametric analysis. The validation of the numerical model was carried out based on the

experimental results of the in-plane walls accordance with Sec. 2.

3.1 Modeling approach

Masonry material is heterogeneous and anisotropic material due to different constituent materials such as mortar, unit and presence of mortar joints in two directions. Macro and micro methods are developed by researchers for masonry.

The macro model is based on the homogeneous material and it can provide an approximate response only for a basic design. In micro modeling, units, mortar and unit/mortar interface are represented by continuous and discontinuous elements, respectively. Although this approach is more realistic and can predict the local behavior of masonry, modeling becomes a complicated question by considering all behaviors of the masonry constituent and this makes the heterogeneous approach uneconomical and inefficient in terms of time. To overcome this problem, simplified micro modeling has been established and most studies have been conducted on masonry finite element modeling. In this approach, mortar joints are tied into the unit/mortar interface as a discontinuous element. Expanded units up to half of the mortar thickness in vertical and horizontal directions were simulated to continuous elements (Dolatshahi 2012, Lourenço 1997, Bolhassani *et al.* 2015, Milani *et al.* 2009).

In this study, the simplified micro modeling approach was chosen for the simulation because it includes all basic failure mechanisms that characterize masonry, enabling the detailed representation of resisting mechanisms of the walls.

3.2. materials model and model inputs

3.2.1 materials model

The Concrete Damaged Plasticity (CDP) model proposed by ABAQUS software was used to model the non-linear behavior (tension and compression) of those materials (see Fig. 7(a)). This model enables to investigate the non-linear behavior of isotropic softening materials under static and dynamic loads. It is also suitable for modeling materials with distinct tensile and compressive strength, and damage parameters. The two damage

parameters used are called d_t and d_c , the first referred to tension and the latter to compression. They can vary between 0 (undamaged state) and 1 (totally damaged state) and modify the uniaxial stress–strain behavior in the unloading path, penalizing the stiffness of the descending branch by means of the well-known Hooke's law as $\sigma_{t,c}=(1-d_{t,c})E_0(\varepsilon_{t,c}-\varepsilon_{t,c}^{plc})$. In this relationship, σ_t and σ_c are the uniaxial tensile and compressive stresses, E_0 is the initial elastic modulus (undamaged state), ε_c and ε_t are the total strain in compression and tension and ε_c^{plc} (ε_t^{plc}) are the total plastic strains in compression (tension). The model assumes that the two main failure mechanisms are tensile cracking and compressive crushing (Bertolesi *et al.* 2014). The plasticity behavior of both ECC mortar and expanded masonry units in compression was modeled using the Drucker-Prager plasticity model (ABAQUS 2013).

Generally, cohesive interactions are a function of displacement separation between the edges of potential cracks. The mechanical constitutive behavior of cohesive elements can be defined in three methods: (1) uniaxial stress-based, (2) continuum based and (3) traction–separation constitutive model. Where two bodies are connected by a third part material like glue, the continuum based modeling is appropriate for the adhesive. In this case, glue should be considered with a finite thickness. The mechanical properties of adhesive material were employed directly in the model from the experimental results. In general, the adhesive material has more impact than the surrounding material in real structures. The traction–separation constitutive models can also be used when the glue is very thin and for the practical purpose may be considered as a zero thickness material. The traction–separation behavior of the cohesive element was employed to model the joint interfaces in a simplified masonry micro model (interfaces between expanded masonry units). A typical traction–separation response is presented in Fig. 7(b). In the elastic part, the traction stress vector consists of normal, t_n and two shear traction components, t_s and t_t . These components represent mode I, II and III of fracture modes shown in Fig. 7(b). Also in this model d_n , d_s and d_t represent the corresponding initial separation caused by pure normal, in plane and out-of-plane shear stresses, respectively. These values can be calculated using the stiffness and strength of each fracture mode. The second part of traction–separation response shows the damage propagation of bond which can be determined in different ways. The normal equivalent stiffness, $k_{nn}=(E_b \times E_m)/(t_m \times (E_b - E_m))$, is expressed as a function of the mortar's moduli of elasticity (E_m) and unit's moduli of elasticity (E_b), and the thickness of the mortar (t_m). To calculate the shear equivalent stiffness (k_{ss} and k_{tt}), the shear moduli replace the moduli of elasticity (Bolhassani *et al.* 2015). Coulomb frictional contact behavior is used to bond two bodies, degraded due to the tensile or shear deformation. Coulomb friction describes the interaction of contacting surfaces and the model characterizes the frictional behavior, using a coefficient of friction, μ . It is important to avoid components penetration after forming the contact, especially for the normal behavior of contacts. This allows the assemblages to take apart in presence of the

critical force. ABAQUS provides two options for the standard contact including surface-to-surface and self-contact. For the present study, surface-to-surface contact was used and contacting properties for the tangential and normal behavior were specified. This contact is applicable for modeling two surfaces that are deformable. The coefficient of friction can be defined based on slip-rate data. In this study, contact-pressure dependent behavior was used based on the results from the triplet shear test.

3.2.2 model inputs

The material properties which were used for defining the CDP model parameters of masonry and ECC materials were obtained by the materials experiments, presented in Sec. 2.1.1. The compressive behavior of CDP masonry model was extracted from stress–strain curves prisms, presented in Fig. 2(d). Also, the tensile and compressive behavior of CDP model for ECC mortar were extracted from stress–strain curves, presented in Fig. 1(b) and 1(d), respectively. Elasticity modulus of masonry and ECC materials are 4900 and 10400 MPa, respectively. In the absence of plasticity parameters, they were indirectly determined by trial and error and by use of common values recommended in the literature (ABAQUS 2013, Bolhassani *et al.* 2015, Maalej and Leong 2005). So, plasticity parameters including eccentricity, f_b/f_c , K coefficient and viscosity parameter have been assumed 0.1, 1.16, 0.67 and 0.001, respectively. Also, dilation angle of ECC and masonry materials have been assumed 10 and 32, respectively. Cohesive element behavior of cement mortar including tangential behavior, normal behavior, stiffness coefficients and damage propagation of bond were defined based on information presented in Table 2. These information is calculated by the experimental results and the relationships presented in Sec. 3.2.1. Based on the experimental results, the friction coefficient, Elasticity modulus of clay brick and cement mortar materials have been obtained 0.91, 19400MPa and 6323MPa, respectively. Also, Normal traction stress, Interface cohesion (shear I and shear II) and plastic displacement have been obtained 1.4MPa, 0.25MPa and 0.02mm, respectively.

3.3 Finite element modeling and analysis

The expanded units and ECC layer were modelled using eight node linear brick elements (3D hexahedral shaped) with reduced integration (type C3D8R) (ABAQUS 2013).

The joint interfaces were modelled based on a surface-based cohesive approach. The contacts between adjacent masonry units were defined through a node to surface discretization method with finite sliding formulation.

Hard contact behavior was defined between the adjacent surfaces of masonry units by the contact pressure-overclosure relationship. The boundary conditions of the model and between the elements were considered in accordance with the experimental observations. Due to the fact that deboning did not occurred between the ECC layer and the wall, the TIE method was used. Dowel rebars were modelled through embedded bars.

According to experimental observations, rebar strains were computed from the displacement field of the

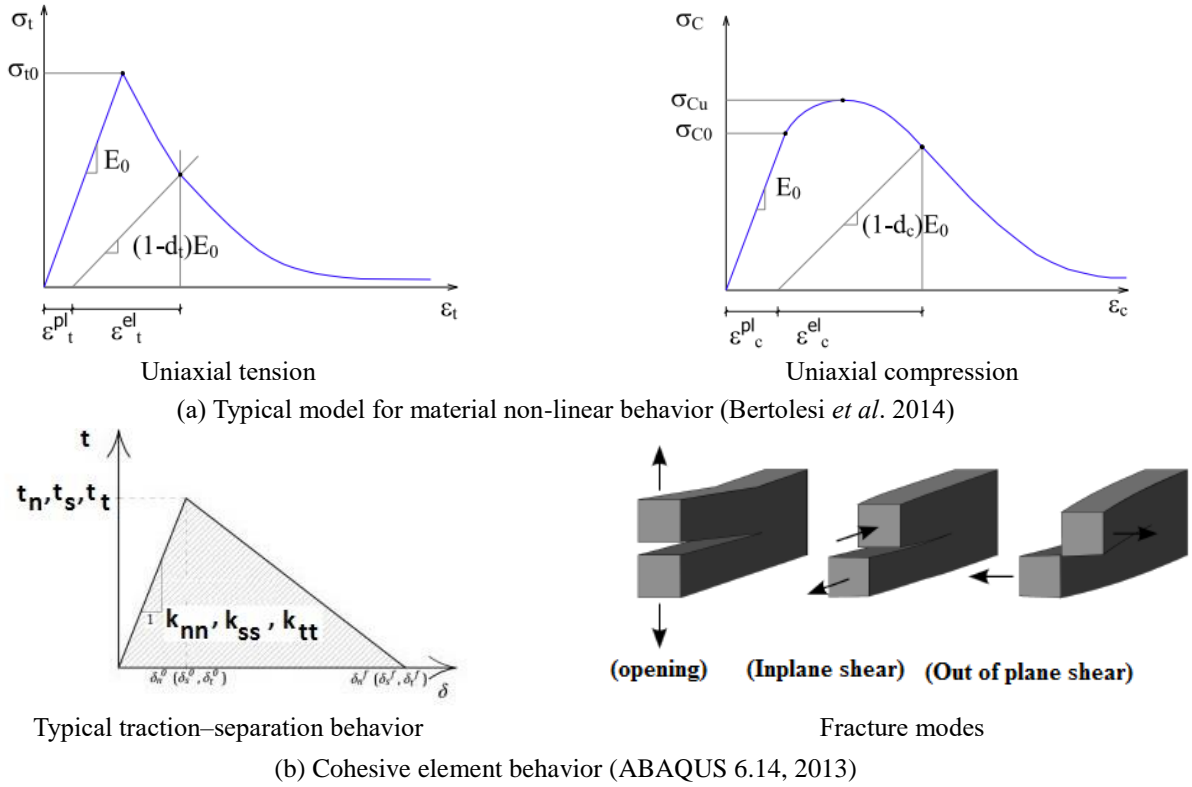


Fig. 7 Typical model for material non-linear behavior and cohesive element behavior

Table 2 Cohesive element characteristic (experimental results)

Tangential behavior	Normal behavior	Stiffness coefficients (N/mm ³)			Damage (MPa)			
		k _{nn}	k _{ss}	k _{tt}	Normal	Shear I	Shear II	Plastic dis.(mm)
0.91	Hard contact	469	187	187	1.4	0.25	0.25	0.02

continuous elements (structural elements), meaning that a perfect bond between the reinforcement and the surrounding ECC layer and concrete foundation was adopted. All models were tested under displacement control by applying displacement at the top of the specimen using ABAQUS explicit.

3.4 Validation of numerical model

In Fig. 8(a), a comparison between experimental hysteretic loop envelopes and lateral strength–relative displacement numerical envelope is illustrated.

It is observed that the force–displacement numerical envelope fits the experimental monotonic envelope very well, both in terms of maximum lateral resistance and initial stiffness. The maximum difference between experimental and numerical lateral strength is about 10%. In addition, the wall shear strength in both experimental and numerical methods decreased at the same drift. Having decreased the shear strength, the form of the numerical curve differed from that of the experimental curve in the retrofitted wall. This difference was more significant at the positive area of the curves. This may be due to the difference between the numerical (pushover) and experimental (cyclic) loading types. At the end of loading process, the amounts of wall

shear strength were in good agreement in both methods.

As shown in Fig. 8(b) and 8(c), the retrofitted URM wall failure mode and the cracking pattern of masonry and the ECC layer are in good agreement with experimental observations. According to these figures, the ECC layer was ruptured at the top of the steel rebar dowels. The damage to the masonry also included the bed joint sliding and limited crushing of the bricks at the wall toe.

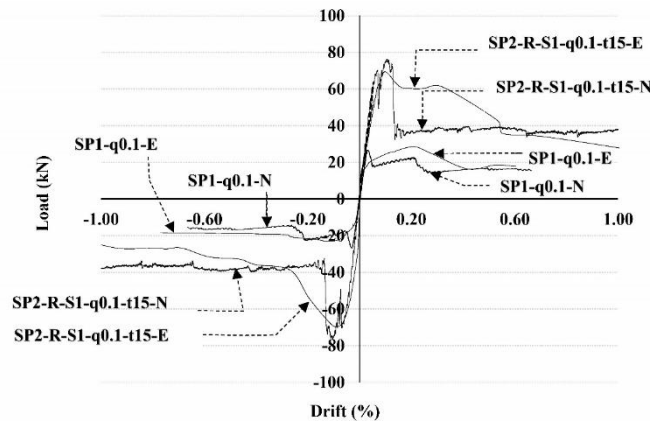
4. Parametric analysis

Having validated the numerical model, a parametric analysis was performed for the assessment of the influence of different parameters on the lateral strength of the retrofitted URM walls.

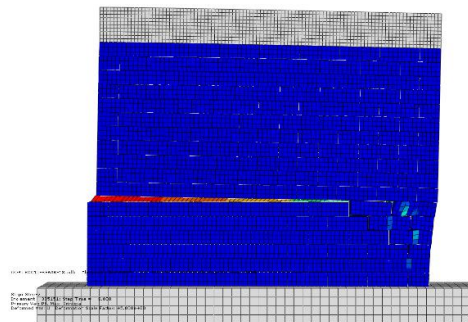
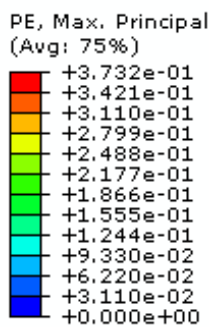
- In this study, three types of parameters have been investigated: variation of pre-compression level as 0.1, 0.5 and 1MPa, one or both sides retrofitting on the URM wall and, variation of ECC layer thickness as 10, 15, 20 and 30 mm.

(a)Variation of Pre-compression and one or both sides retrofitting

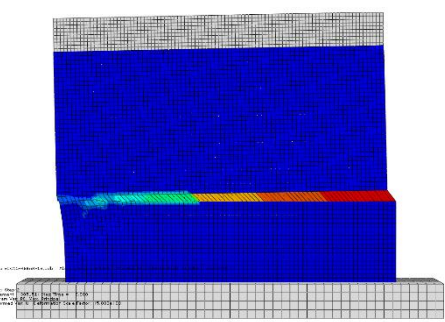
- The lateral capacity of the retrofitted URM under the pre-compressive stress of 0.1, 0.5 and 1MPa was



(a) Lateral load vs. relative displacement diagrams



(b) Plastic strain in masonry side



(c) Plastic strain in ECC side

Fig. 8 Validation of numerical results

calculated numerically. In this study, the other wall characteristics and its retrofitted details, including the thickness of the ECC layer ($t_{ECC}=15$ mm), were similar to the experimental specimen. Also, one or both sides retrofitting on the URM wall has been investigated. The force–displacement numerical curve and the cracking pattern of the URM wall and material (ECC and masonry unites) plastic strain have been illustrated in Fig. 9.

As shown in Fig. 9(a), the lateral wall capacity changes relative to the pre-compression levels indicate that, with increasing pressure, the effect of ECC mortar on the retrofitted wall lateral capacity decreased. The specimens numbering is in the form of “SP-R-S-q-t-E or N” where SP=number of specimens, R=retrofitted specimen, S=one or both sides retrofitting, t=thickness of the ECC layer, q=vertical pre-compression stress and E or N=experimental or numerical method, respectively.

one-way or two-way ECC mortar has not changed the failure pattern of wall. As shown in Fig. 9(a), the increased amount of retrofitted URM lateral capacity is approximately twice the lateral capacity of the ECC layer.

Also according to Fig. 9(b) and 9(c), the increase in compression stress on the foot of the wall caused a toe crashing failure mode. This is because of the negligible influence of ECC mortar on the compressive strength of masonry materials.

(b) Variation of ECC layer thickness

In this section, the lateral capacity of the retrofitted

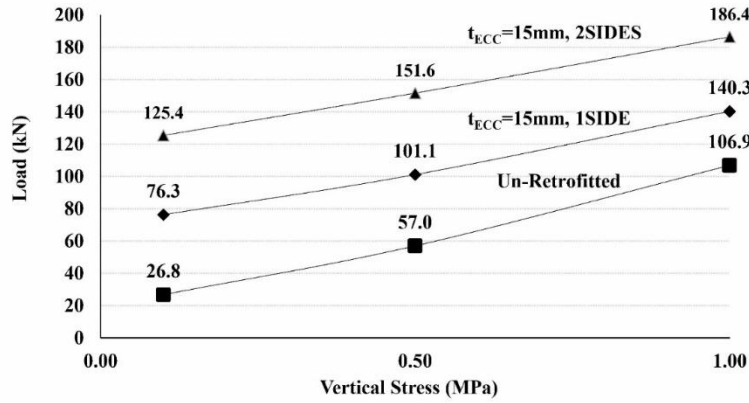
URM is determined by changing the ECC layer thickness of the of 10, 15, 20 and 30mm. The other wall characteristics and its retrofitted details, including the pre-compressive stress, are similar to those of the experimental specimen.

As shown in Fig. 10, the retrofitted URM wall failure mode and the cracking pattern of masonry and the ECC layer ($t_{ECC}=30$ mm) are similar to those of the experimental specimen.

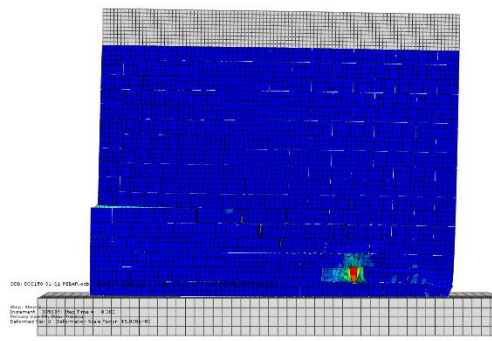
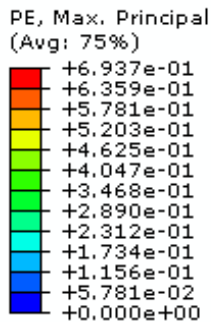
Fig. 10(a) compares the strength increase with the number of ECC layers applied on a URM wall, showing that as additional ECC layer was applied, the ratio of strength increase to the number of ECC layers is increased.

5. Estimating lateral capacity

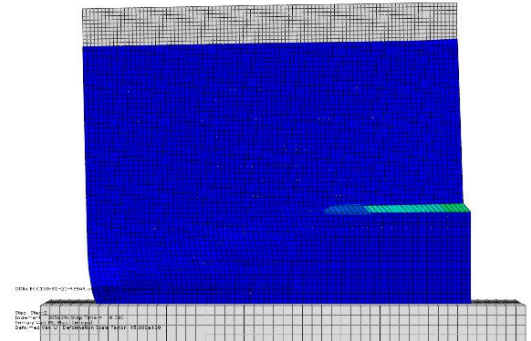
In this section, according to the experimental observations and numerical obtained results, a relationship for estimating the masonry wall lateral capacity, retrofitted with ECC mortar, has been presented. This relationship has been proposed for the conditions where the ECC layer is connected to the wall foundation through steel rebar dowels. The retrofitted wall has been modelled like a composite element, including the bearing URM wall and the ECC layer. The distribution of forces on the retrofitted wall is in accordance with Fig. 11(a) and 11(b). According to experimental observations, the retrofitted wall has been affected by the bending action. Based on the equations of



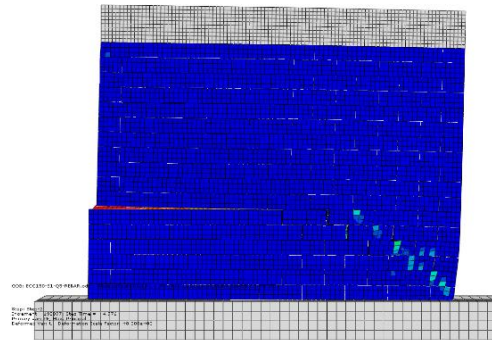
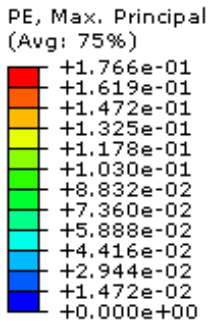
(a) Lateral load vs. vertical stress



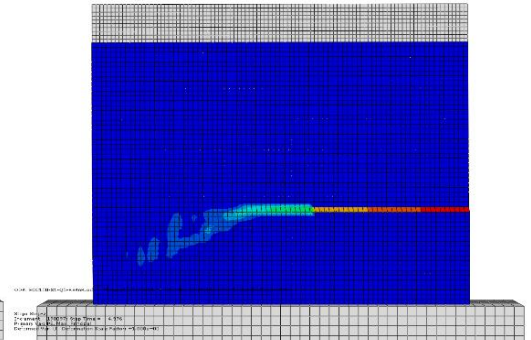
(b) Plastic strain in masonry side (q=1MPa)



(c) Plastic strain in ECC layer side (q=1MPa)



(d) Plastic strain in masonry side (q=0.5MPa)

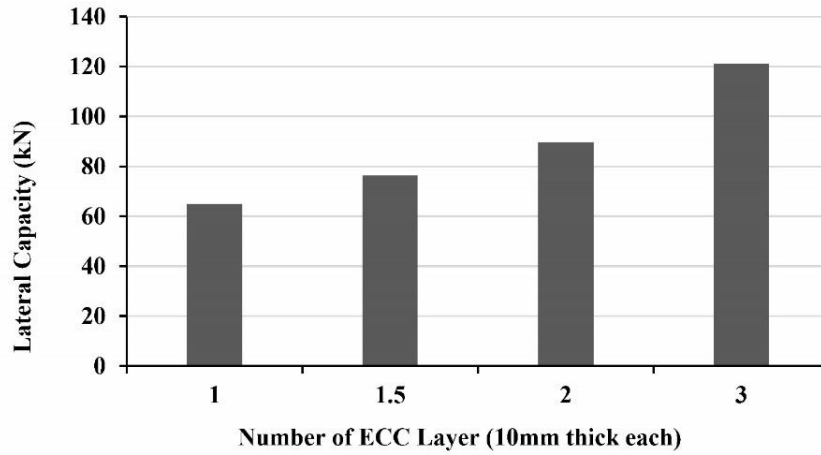


(e) Plastic strain in ECC layer side (q=0.5MPa)

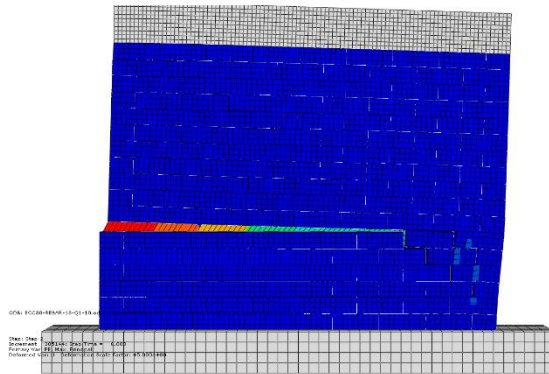
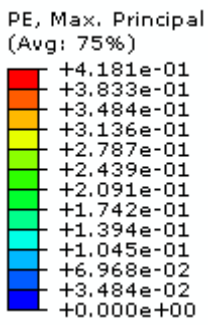
Fig. 9 Influence of pre-compression in lateral strength of retrofitted URM wall

equilibrium, the maximum amount of the retrofitted wall shear strength (V_{max}) can be calculated according to Eq. (1), where H_1 and M_{max} are the wall height from the top of steel rebar dowels and the retrofitted wall flexural capacity, respectively. The retrofitted wall flexural capacity can be calculated by means of a simple flexure theory, based on the assumption that the plane sections remain plane after bending. Based on experimental observations, no slip and debonding between the ECC layer and the masonry wall happened. Therefore, the strain amount was the same for both elements. The retrofitted wall flexural capacity has been calculated based on the ultimate tensile strain of the ECC layer (ϵ_{tuECC}). Of course, the retrofitted wall ultimate compressive strain (ϵ_c) should not be greater than neither the ultimate compressive strain of masonry materials (ϵ_{cum}) nor that of the ECC layer (ϵ_{cuECC}). The retrofitted wall flexural capacity has been calculated according to Fig. 11

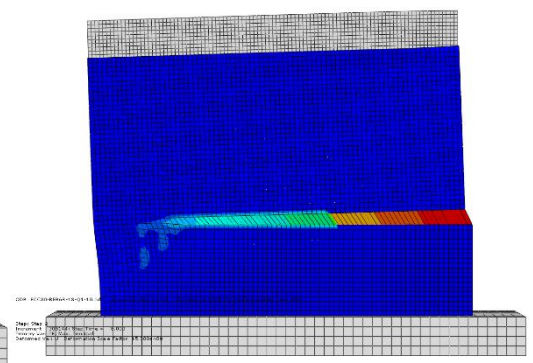
and the Eq. (2) - (3), where t_{ECC} =ECC layer thickness, t_m =masonry wall thickness, l_w =wall effective length equal to 0.8 of the wall actual length (L_w), N =wall axial force, f_{tuECC} =ECC mortar ultimate tensile stress, E_{ECC} =ECC mortar modulus elasticity and E_m =masonry prism modulus elasticity. The wall effective length (l_w) was chosen in accordance with the recommended relationship for calculating the shear walls bending capacity, presented in ACI 318-008, (2008). The compressive strain (ϵ_c) is determined in terms of the neutral axis depth considering the similar triangles of the strain diagram presented in Fig. 11(c). According to Fig. 1, the direct tensile and compressive test have been used to determine characteristics of the ECC layer. The tensile strength of the masonry wall has been ignored to calculate the flexural capacity of the retrofitted wall.



(a) Lateral load vs. ECC layer thickness

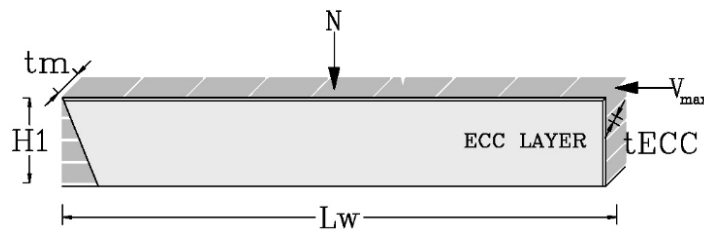


(b) Plastic strain of masonry side

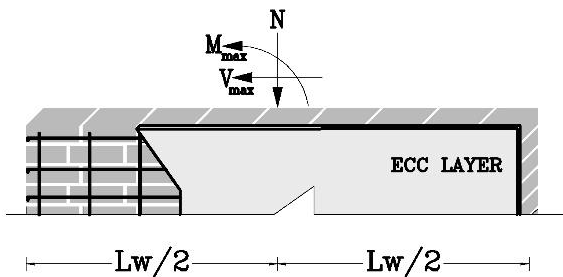


(c) Plastic strain of ECC layer

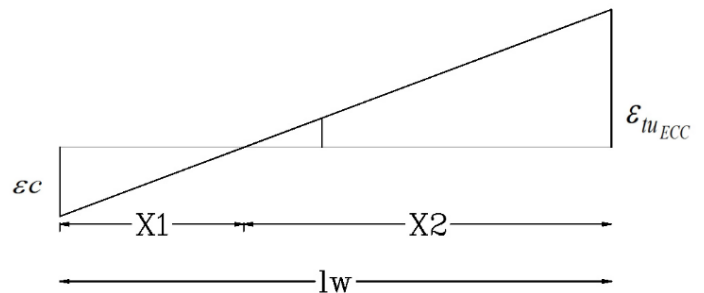
Fig. 10 Influence of ECC layer thickness in lateral strength of URM wall ($t_{ECC}=30$ mm, $q=0.1$ MPa)



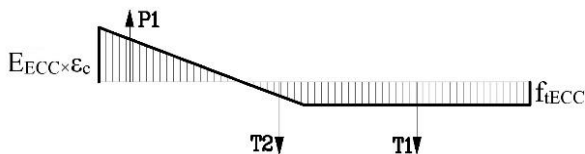
(a) Applied forces on top of the retrofitted wall



(b) Wall internal forces above the steel rebar dowels



(c) Linear strain variation along the retrofitted wall



(d) Stress variation in ECC along the retrofitted wall



(e) Compressive stress variation in the masonry wall

Fig11. Retrofitted wall modeling

Table 3 Comparison of calculated and measured shear capacity

q (MPa)	t _{ECC} (mm)	Side of retrofiting	V _{N,max} (kN)	V _{C,max} (kN)	V _{C,max} /V _{N,max}
0.1	15	1S	76	70	0.92
0.1	15	2S	125	119	0.95
0.5	15	1S	101	118	1.17
0.5	15	2S	152	161	1.06
1.0	15	1S	140	168	1.20
1.0	15	2S	186	208	1.12
0.1	10	1S	65	53	0.82
0.1	20	1S	90	87	0.97
0.1	30	1S	121	119	0.98
0.1	15	1S	76	70	0.92

Note: V_{N, max}= numerical maximum shear strength; V_{c, max}= calculated maximum shear strength

6. Comparison of calculated and measured shear capacity

The comparison of numerical and proposed relationships results have been presented in Table 3. It is shown that the difference between the results of both methods is about 20%.

$$V_{\max} = \frac{M_{\max}}{H_1} \quad (1)$$

$$\sum M = \sum F_i X_i - V_{\max} \times H_1 = 0 \quad (2)$$

$$\sum F_i = N + T_1 + T_2 - P_1 - P_2 = 0 \quad (3)$$

7. Conclusions

In this study, the effect of Engineered Cementitious Composites (ECC) on the lateral strength of a bearing unreinforced Masonry (URM) wall, was experimentally and numerically investigated. Two half scale solid walls were constructed and tested under quasi-static lateral loading.

In the retrofitted specimens, the ECC layer was connected to the wall foundation using steel rebar dowels. The effect of the pre-compression levels, variations of the ECC layer thickness and one or both sides retrofiting, on the URM wall lateral strength was numerically investigated. The following results were obtained:

- According to experimental observation, Connecting the ECC layer to the wall foundation was effective in preventing the uplifting phenomena and the increase in wall shear strength. The experimental results indicated a 175% increase in the lateral strength of the retrofitted wall compared to that of the reference wall. According to the numerical results, the amount of lateral strength was obtained as 145%, 240% and 350% for 10, 20 and 30 mm ECC layer thicknesses, respectively.
- In experimental specimen, there was no debonding

between the ECC layer and the masonry wall. Therefore, the bonding between the ECC layer and the masonry wall can be assured for the conditions of this research.

- The numerical results indicated that increase in the pre-compression levels reduced the influence of the ECC mortar on the wall lateral strength. This led to rocking (flexural behavior) along with toe-crushing failure modes.
- The results indicated when the ECC mortar is applied on both sides of the wall, the wall lateral strength can be significantly improved.
- Based on the experimental observations and numerical results, relationships were developed to estimate the retrofitted wall shear strength. The results of this method were in good agreement with the experimental results.

Acknowledgements

The authors acknowledge the assistance of laboratory staff of material and structural engineering departments of Building and Housing Research Center (B.H.R.C), Tehran, Iran. The authors also like to thank Mr. Mansoor Jamee for his help in carrying out the experiments.

References

- ABAQUS (2013), "Online documentation", SIMULIA Inc.
- ACI 318-08 (2008), "Building code requirements for structural concrete and commentary", American Concrete Institute.
- ACI/440.7R. (2010), "Guide for the design and construction of externally bonded fiber-reinforced polymer systems for strengthening un-reinforced masonry structures", *American concrete institute (ACI)*.
- AL-Gemeel, A. and Zhuge, Y. (2018), "Experimental investigation of textile reinforced engineered cementitious composite (ECC) for square concrete column confinement", *Construct. Build. Mat.*, **174**(20), 594-602. <https://doi.org/10.1016/j.conbuildmat.2018.04.161>.
- ASCE/41-17 (2017), "Seismic evaluation and retrofit of existing buildings", Reston, Virginia, 20191-4382: American Society of Civil Engineers.
- ASTM-C1314-16 (2016), "Standard test method for compressive strength of masonry prisms", *West Conshohocken*.
- ASTM-C270-07 (2007), "Standard specification for mortar for unit masonry", *West Conshohocken*.
- ASTM-C469-14 (2002), "Standard test method for static modulus of elasticity and poisson's ratio of concrete in compression", *West Conshohocken*.
- ASTM-C67-14 (2014), "Standard test methods for sampling and testing brick and structural clay tile", *West Conshohocken*.
- ATC 24 (1992), "Guidelines for cyclic seismic testing of components of steel structures", *Applied Technology Council*, Redwood City.
- Basilio, I., Fedele, R., Lourenço, P.B. and Milani, G. (2014), "Assessment of curved FRP-reinforced masonry prisms: experiments and modeling", *Construct. Build. Mat.*, **51**, 492-505. <https://doi.org/10.1016/j.conbuildmat.2013.11.011>.
- Bernat-Maso, E., Gil, L. and Roca, P. (2015), "Numerical analysis of the load-bearing capacity of brick masonry walls strengthened with textile reinforced mortar and subjected to eccentric compressive loading", *Eng. Struct.*, **91**, 96-111.

- <https://doi.org/10.1016/j.engstruct.2015.02.032>.
- Bertolesi, E., Carozzi, F.G., Milani, G. and Poggi, C. (2014), "Numerical modeling of Fabric Reinforce Cementitious Matrix composites (FRCM) in tension", *Construct. Build. Mat.*, **70**, 531-548. <https://doi.org/10.1016/j.conbuildmat.2014.08.006>.
- Bilgin, H. and Huta, E. (2018), "Earthquake performance assessment of low and mid-rise buildings: Emphasis on URM buildings in Albania", *Earthq. Struct.*, **14**(6), 599-614. <https://doi.org/10.12989/eas.2018.14.6.000>.
- Bolhassani, M., Hamid, A., Lau, A. and Moon, F. (2015), "Simplified micro modeling of partially grouted masonry assemblages", *Construct. Build. Mat.*, **83**, 159-73. <https://doi.org/10.1016/j.conbuildmat.2015.03.021>.
- Carozzi, F., Milani, G. and Poggi, C. (2014), "Mechanical properties and numerical modeling of Fabric Reinforced Cementitious Matrix (FRCM) systems for strengthening of masonry structures", *Compos. Struct.*, **107**, 711-725. <https://doi.org/10.1016/j.compstruct.2013.08.026>.
- Carozzi, F.G., Poggi, C., Bertolesi, E. and Milani, G. (2018), "Ancient masonry arches and vaults strengthened with TRM, SRG and FRP composites: Experimental evaluation", *Compos. Struct.*, **187**(1), 466-480. <https://doi.org/10.1016/j.compstruct.2017.12.075>.
- Darbhanzi, A., Marefat, M.S., Khanmohammadi, M., Moradimanesh, A. and Zare, H. (2018), "Seismic performance of retrofitted URM walls with diagonal and vertical steel strips", *Earthq. Struct.*, **14**(5), 449-458. <https://doi.org/10.12989/eas.2018.14.5.449>.
- Dehghani, A., Fischer, G. and Alahi, F.N. (2015), "Strengthening masonry infill panels using engineered cementitious composites", *Mat. Struct.*, **48**(1-2), 185-204. <https://doi.org/10.1617/s11527-013-0176-4>.
- Deng, M. and Yang, S. (2018), "Cyclic testing of unreinforced masonry walls retrofitted with engineered cementitious composites", *Construct. Build. Mat.*, **177**, 395-408. <https://doi.org/10.1016/j.conbuildmat.2018.05.132>.
- Dolatshahi, K.M. (2012), "Computational, analytical and experimental modeling of masonry structures", *State Univ. New York at Buffalo*.
- ElGawady, M., Lestuzzi, P. and Badoux, M. (2007), "Static cyclic response of masonry walls retrofitted with fiber-reinforced polymers", *J. Compos. Construct.*, **11**(1), 50-61. [https://doi.org/10.1061/\(ASCE\)1090-0268\(2007\)11:1\(50\)](https://doi.org/10.1061/(ASCE)1090-0268(2007)11:1(50)).
- EN-12390-3 (2009), "Testing hardened concrete - part 3: compressive strength of test specimens", *European Committee for Standardization*, Brussels, Belgium.
- EN 1052-3 (2007), "Methods of test for masonry, Part 3: determination of initial shear strength", *European Standard*.
- FEMA-F.461 (2007), "Interim protocols for determining seismic performance characteristics of structural and nonstructural components through laboratory testing", Federal Emergency Management Agency, Redwood City.
- Ghiassi, B., Soltani, M. and Tasnimi, A. (2011), "Seismic evaluation of masonry structures strengthened with reinforced concrete layers", *J. Struct. Eng.*, **138**(6), 729-743. [https://doi.org/10.1061/\(ASCE\)ST.1943-541X.0000513](https://doi.org/10.1061/(ASCE)ST.1943-541X.0000513).
- Hung, C. and Chen, Y. (2016), "Innovative ECC jacketing for retrofitting shear-deficient RC members", *Construct. Build. Mat.*, **111**(15), 408-418. <https://doi.org/10.1016/j.conbuildmat.2016.02.077>.
- Ismail, N., El-Maaddawy, T. and Khattak, N. (2018), "Quasi-static in-plane testing of FRCM strengthened non-ductile reinforced concrete frames with masonry infills", *Construction and building materials*, **186**, 1286-1298.
- ISO-16670:2003 (2003), "Timber structures – joints made with mechanical fasteners - quasi-static reversed cyclic test method", ISO 14443, *International Organization for Standardization* Geneva, Switzerland.
- JSCE2008 (2008), "Recommendation for design and construction of high performance fiber reinforced cement composites with multiple fine cracks", *Jpn. Soc. Civ. Eng.*
- Kadam, S., Singh, Y. and Li, B. (2014), "Strengthening of unreinforced masonry using welded wire mesh and micro-concrete-Behaviour under in-plane action", *Construct. Build. Mat.*, **54**(15), 247-257. <https://doi.org/10.1016/j.conbuildmat.2013.12.033>.
- Kesner, K. and Billington, S.L. (2004), "Tension, compression and cyclic testing of engineered cementitious composite materials", *MCEER*.
- Kota, S.K., Rama, J.S. and Murthy, A.R. (2019), "Strengthening RC frames subjected to lateral load with Ultra High-Performance fiber reinforced concrete using damage plasticity model", *Earthq. Struct.*, **17**(2), 221-232. <https://doi.org/10.12989/eas.2019.17.2.221>.
- Krawinkler, H. (2009), "Loading histories for cyclic tests in support of performance assessment of structural components", *In the 3rd International Conference on Advances in Experimental Structural Engineering*, San Francisco. U.S.A.
- Kyriakides, M.A. and Billington, S.L. (2014), "Behavior of unreinforced masonry prisms and beams retrofitted with engineered cementitious composites", *Mat. Struct.*, **47**(9), 1573-1587. <https://doi.org/10.1617/s11527-013-0138-x>.
- Liang, X. and Xing, P. (2018), "Seismic behavior of fiber reinforced cementitious composites coupling beams with conventional reinforcement", *Earthq. Struct.*, **14**(3), 261-271. <https://doi.org/10.12989/eas.2018.14.3.261>.
- Lin, Y., Lawley, D., Wotherspoon, L. and Ingham, J. (2016), "Out-of-plane testing of unreinforced masonry walls strengthened using ECC shotcrete", *Struct.*, **7**, 33-42. <https://doi.org/10.1016/j.istruc.2016.04.005>.
- Lin, Y., Wotherspoon, L., Scott, A. and Ingham, J. (2014), "In-plane strengthening of clay brick unreinforced masonry wallettes using ECC shotcrete", *Eng. Struct.*, **66**(1), 57-65. <https://doi.org/10.1016/j.engstruct.2014.01.043>.
- Lourenço, P.J. (1997), "Computational strategies for masonry structures", Master Thesis, *Delft University of Technology*, Portugal.
- Luccioni, B. and Rougier, V. (2011), "In-plane retrofitting of masonry panels with fibre reinforced composite materials", *Construct. Build. Mat.*, **25**(4), 1772-1788. <https://doi.org/10.1016/j.conbuildmat.2010.11.088>.
- Maalej, M. and Leong, K. (2005), "Engineered cementitious composites for effective FRP-strengthening of RC beams", *Compos. Sci. Technol.*, **65**(7-8), 1120-8. <https://doi.org/10.1016/j.compscitech.2004.11.007>.
- Maalej, M., Lin, V., Nguyen, M. and Quek, S. (2010), "Engineered cementitious composites for effective strengthening of unreinforced masonry walls", *Eng. Struct.*, **32**(8), 2432-2439. <https://doi.org/10.1016/j.engstruct.2010.04.017>.
- Maso, E.B., Escrig, C., Chrysl, A.A. and Lluís, G. (2014), "Experimental assessment of textile reinforced sprayed mortar strengthening system for brickwork wallettes", *Construct. Build. Mat.*, **50**, 226-236. <https://doi.org/10.1016/j.conbuildmat.2013.09.031>.
- Milani, G., Milani, E. and Tralli, A. (2009), "Upper Bound limit analysis model for FRP-reinforced masonry curved structures. Part I: Unreinforced masonry failure surfaces", *Comput. Struct.*, **87**(23-24), 1516-1533. <https://doi.org/10.1016/j.compstruc.2009.07.007>.
- Nezhad, R., Kabir, M. and Banazadeh, M. (2016), "Shaking table test of fibre reinforced masonry walls under out-of-plane loading", *Construct. Build. Mat.*, **120**, 89-103. <https://doi.org/10.1016/j.conbuildmat.2016.05.097>.
- Popa, V., Pascu, R., Papurcu, A. and Albotă, E. (2016),

- “Retrofitting of squat masonry walls by FRP grids bonded by cement-based mortar”, *Earthq. Struct.*, **10**(1), 125-139. <https://doi.org/10.12989/eas.2016.10.1.125>.
- Singh, S., Patil, R. and Munjal, P. (2017), “Study of flexural response of engineered cementitious composite faced masonry structures”, *Eng. Struct.*, **150**(1), 786-802. <https://doi.org/10.1016/j.engstruct.2017.07.089>.
- Triantafillou, T. (2011), “Innovative textile-based composites for strengthening and seismic retrofitting of concrete and masonry structures”, *In Advances in FRP composites in civil engineering; springer, Berlin, Heidelberg*, 3-12.
- Ural, A. (2013), “19th May 2011 Simav (Kütahya) earthquake and response of masonry Halil Aga Mosque”, *Earthq. Struct.*, **4**(6), 671-683. <https://doi.org/10.12989/eas.2013.4.6.671>.
- Vanin, A. and Foraboschi, P. (2012), “In-plane behavior of perforated brick masonry walls”, *Mat. Struct.*, **45**(7), 1019-1034. <https://doi.org/10.1617/s11527-011-9814-x>.
- Yardim, Y. and Lalaj, O. (2016), “Shear strengthening of unreinforced masonry wall with different fiber reinforced mortar jacketing”, *Construct. Build. Mat.*, **102**, 149-154. <https://doi.org/10.1016/j.conbuildmat.2015.10.095>.

AT